Rings in central-force network dynamics

F. L. Galeener* and M. F. Thorpe†
Xerox Palo Alto Research Center, 3333 Coyote Hill Road, Palo Alto, California 94304
(Received 5 July 1983)

The central-force network dynamics model for glasses is extended to treat networks involving small regular rings of bonds. In particular, band-limit formulas are obtained for an A_2X_3 glass consisting of regular puckered six-membered A_3X_3 rings. The special case of *planar* rings is compared with observations on vitreous B_2O_3. This continuous random network of "boroxol" rings shows improved agreement with experiment over a model not containing rings. The remaining discrepancies illustrate the need to include noncentral forces in the network dynamics of v-B_2O_3.

I. INTRODUCTION

In this paper we illustrate methods for extending the central-force dynamics of glasses from the relatively simple topologies used by Sen and Thorpe[1] and Thorpe and Galeener[2] to related topologies which contain regular rings of bonds. Specifically, we present formulas for the band limits of a homogeneous A_2X_3 continuous random network of arbitrarily puckered regular six-membered rings, and note the influence of the rings on the vibrational density of states. We emphasize some aspects of the special case of *planar* rings, in order to compare with experimental data on vitreous (v-) B_2O_3. In the case of v-B_2O_3, we conclude that the rings lead to much improved agreement with experiment, but that further extensions to include noncentral forces are warranted.

A. Rings in amorphous solids

A small body of theoretical work has been developed concerning the effects of rings of bonds on the *electronic* properties of disordered or amorphous (a-) solids.[3–6] It is clear that completed rings of bonds must exist in all network glasses, and the statistics of rings have been counted[7] for several ball-and-stick structure models, including the Bell and Dean model[8] for vitreous (v-) SiO_2, the Polk model[9] for a-Ge, and the Connell-Temkin model[10] for a-Si. There have been few, if any, unambiguous observations of electronic properties of amorphous materials that are due to these rings. For example, the effect of fivefold rings on the electronic structure of a-Si has been reported,[3,4] but the observed effect is small and the interpretation is ambiguous. It has also recently been suggested[5] that odd-membered rings are important in determining the band gap in a-Si; however, it has not been possible to detect the existence of such rings (e.g., fivefold) in the radial distribution function of a-Si.[11] Completed rings also must exist in crystalline materials, and it is easy to determine their statistics from the definitive structural data available on a large variety of crystalline materials.[7]

Part of the problem with assessing the role of rings in the properties of amorphous solids is the general lack of definitive structural data defining the statistics and geometry of rings in real amorphous materials. Another problem is that the rings are generally thought to be irregular, containing a wide variation of bond angles in any group of n-fold rings. This situation is exemplified in Fig. 1, which shows schematically the continuous random network model for a 3-2-connected glass, as first proposed by Zachariasen.[12] Here each A atom is surrounded trigonally by three X atoms, and each X atom bridges between two A atoms with an A—X—A angle θ that varies over a large range. This disordered system of corner sharing identical AX_3 "triangles" has exact A_2X_3 stoichiometry and has a wide unspecified variation of ring sizes and configurations.

B. Rings in v-B_2O_3

One likely exception to this complex situation is found in boric oxide glass, v-B_2O_3, for which there is increasing evidence that the structure consists of a network of planar BO_3 triangles, many of them grouped together in threes, to form planar B_3O_3 "boroxol" rings. The situation is illustrated schematically in Fig. 2, where we have shown three kinds of connections between the planar boroxol rings. Here (i) represents a single oxygen atom connecting two rings, with the B—O—B angle θ generally different from site (i) to another similar site. A "dihedral" angle δ is also necessary to specify the relative orientation of the two neighboring rings joined at (i), and δ is assumed to vary, perhaps randomly, from site to site. Site (ii) in Fig.

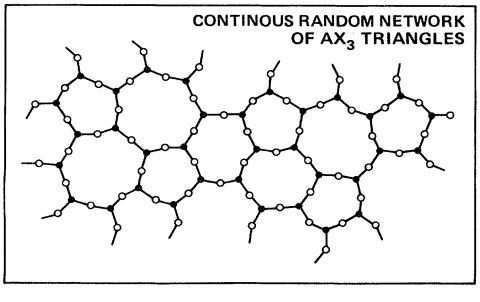

FIG. 1. Schematic (planarized) Zachariasen continuous random network model for the structure of v-B_2O_3. Each boron atom (●) is at the center of an equilateral triangle of oxygen atoms (○), and the (planar) triangles share corners only (not edges) with a large variation in the angles at the bridging oxygen atoms.

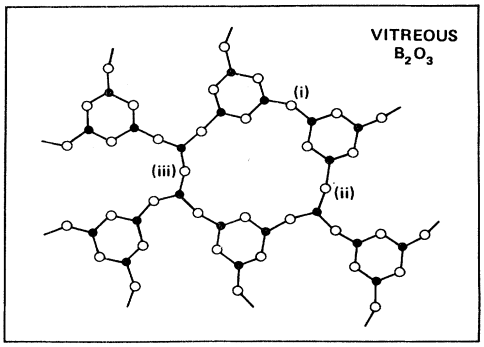

FIG. 2. Schematic (planarized) diagram of the likely network connections in v-B_2O_3, based on B_3O_3 (boroxol) rings. The planar hexagonal units may be connected at their corners by means of a single oxygen bridge (i), a single planar BO_3 triangle (ii), or a pair of such triangles (iii). The angles at the oxygen atoms (○) bridging between planar units (rings or triangles) are assumed to be widely spread, whereas the oxygen angles within the rings are identical at 120°. NMR and diffraction studies conclude that there must be some boron atoms (●) in v-B_2O_3 which are *not* members of boroxol rings.

2 represents the next most complicated connection between rings: three rings joined by a triangle with varying values of θ and δ at the three bridging oxygen atoms involved. Site (iii) represents four rings joined by two triangle units having varying values of θ and δ. Although even larger numbers of rings might be joined by "randomly" oriented triangles, it seems consistent to assume that when three triangles unite they will become planar[13,14] leading to a boroxol ring. The model containing many boroxol rings was first proposed by Goubeau and Keller[15] and was given much support by Krogh-Moe.[16] Mozzi and Warren[17] found that their x-ray radial distribution function (RDF) data on v-B_2O_3 could best be fit by a mixture of independentlv oriented rings and triangles, much like that shown schematically in Fig. 2. Jellison *et al.*[18] have used NMR studies to estimate that 82% of the B atoms are in B_3O_3 rings. The earlier NMR work of Silver and Bray[19] established that *all* BO_3 units are essentially planar.

Elliott[20] has recently questioned the necessity of including boroxyl rings to fit the x-ray RDF data; however, there is a sizable body of other information which points strongly to their existence. The situation up to 1978 is reviewed by Griscom.[21] Very recent neutron-diffraction studies[22] are also best fit by a boroxol-ring model, in which 60% of the B atoms are in boroxol rings.

Important evidence for the existence of boroxol rings in v-B_2O_3 is found in the vibrational spectra. Galeener, Lucovsky, and Mikkelsen[23] have pointed to the *extraordinary* narrowness (15 cm^{-1}) of the dominant Raman line at 808 cm^{-1} as a clear indicator that the B—O—B angles are tightly controlled (±0.8°), as would be the case in boroxol rings. Bell and Carnevale[24] have computer-calculated Raman spectra from a ball-and-stick model containing boroxol rings, and found the boroxol-ring model to better account for the large polarization ratio (I_{HH}/I_{HV}) observed for the dominant Raman line, viz., $I_{HH}/I_{HV}=28$ at 808 cm^{-1}. This latter argument suffers from the fact that the much wider dominant Raman lines in v-SiO_2 and v-GeO_2 show polarization ratios of ~25 and ~50, respectively, yet there is little evidence that these two glasses are composed of tightly regular rings. The bond polarizability calculations of Martin and Galeener[25] for v-GeO_2 would seem to suggest that a large polarization ratio indicates correlated motion over several neighboring structural units in all the glasses mentioned here, including v-B_2O_3.

In summary, there is widespread agreement that v-B_2O_3 consists largely of a network of remarkably regular and planar threefold rings, the so-called boroxol rings known to occur in various alkali-borate crystals,[26] but *not*[21] in crystalline B_2O_3. Since the vibrational properties of "molecular" rings in borate crystals have been modeled extensively,[26] v-B_2O_3 is a good vehicle for exploring the role of rings of network dynamics.

II. CENTRAL-FORCE NETWORK THEORY

A. Network of planar AX_3 triangles

We first consider the simplest possible network model that contains the most certain nearest-neighbor information in v-B_2O_3: that each B atom is at the center of an equilateral triangle of O atoms. (That is, the BO_3 triangles are planar.) We assume that each O atom (of mass m) bridges between two B atoms (of mass M) and that the planar triangles share corners only, not edges. This leads to the idealized network model shown in Fig. 3(a). Here all the O—B—O angles ψ are 120° (planar triangles) and all the bridging oxygen angles are set at a common (most probable) value θ.

To treat vibrations in this system, we use the nearest-neighbor central-force network model, originally introduced by Sen and Thorpe,[1] for AX_2 tetrahedral glasses such as v-SiO_2. In this model, the only basic force acting in the network is along the bond between two nearest neighbors, and is denoted by a force constant α. Other

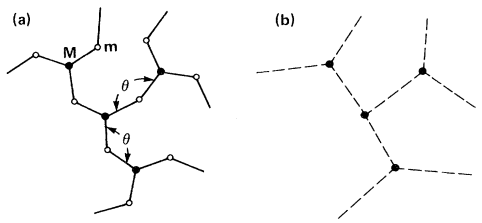

FIG. 3. Local order (a) of an A_2X_3 network of planar triangles that is used to treat vibrations of the Zachariasen model (Fig. 1) in central forces only. The X—A—X angles θ are taken to be the same everywhere, while there is no restriction on the dihedral angle (δ) that determines the relative orientation of two neighbor triangles, given θ. The ring statistics of this network are unspecified. The skeleton network for this structure shows which A atoms interact with one another through a single X-atom bridge, and is shown in (b). The skeleton network determines the connectivity matrix, and the latter plays a central role in setting limits on the allowed vibrational frequencies.

forces, such as intrinsic angle restoring forces, are referred to as noncentral forces, denoted β, and set equal to zero. Galeener[27] has shown the approximate model to have surprising quantitative accuracy (10%) for several AX_2 glasses, and the method was generalized by Thorpe and Galeener[2] to treat several other topologies, including the one now being discussed. In particular, the model was found to explain both the high-frequency infrared modes of AX_2 glasses and the lower-frequency dominant Raman line.[27] This indicated that the absence of noncentral forces β was of secondary importance in v-SiO_2, v-GeO_2, and v-BeF_2. As we shall see, noncentral forces play a more important role when uniform rings are introduced in v-B_2O_3.

Thorpe and Galeener[2] (TG) have shown that the central-force eigenfrequencies of the network in Fig. 3(a) are given by

$$\omega^2=(\alpha/m)+(3\alpha/4M)\pm[(3\alpha/4M)^2+(\alpha\cos\theta/m)^2 -(\alpha^2\cos\theta/2mM)\epsilon]^{1/2}\ , \quad (1)$$

where the ϵ are the eigenvalues of the connectivity matrix of the "skeleton network" (discussed in TG). The skeleton network is formed by drawing straight lines between boron atoms that are connected by a single bridging oxygen atom, and is shown in Fig. 3(b). The skeleton network defines the essential topology of the glass and is paramount in determining the properties of models such as the one discussed in this paper. In the absence of any information about the skeleton network, other than its three-coordinated nature, all we can say[28] is that the eigenvalue spectrum of the connectivity matrix is bounded by

$$-3\le\epsilon\le 3\ . \quad (2)$$

Using these limiting eigenvalues in Eq. (1) leads to four limiting frequencies for the system of triangles, given by

$$\omega_1^2=(\alpha/m)(1+\cos\theta)\ , \quad (3a)$$

$$\omega_2^2=(\alpha/m)(1-\cos\theta)\ , \quad (3b)$$

$$\omega_3^2=(\alpha/m)(1+\cos\theta)+(3\alpha/2M)\ , \quad (3c)$$

$$\omega_4^2=(\alpha/m)(1-\cos\theta)+(3\alpha/2M)\ . \quad (3d)$$

These equations are linear in α and $\cos\theta$, and are plotted as the solid straight lines in Fig. 4(a), using $m/M=m(\mathrm{O})/M(\mathrm{B})=16/11$, as is appropriate for BO_3 triangles. Note that all the variables $(m/\alpha)\omega^2$, $\cos\theta$, and m/M are dimensionless. Since $m>M$, the band edges at ω_2 and ω_3 never cross for any value of θ [just as was the case[1,27] for the tetrahedral glass BeF_2 where $m(\mathrm{F})>M(\mathrm{Be})$]. We have also labeled the limiting frequencies in Fig. 4(a) according to their origin in Eq. (1); for example, -3^+ is obtained by using $\epsilon=-3$ in Eq. (1) and by taking the $+$ choice where $\pm$ appears in Eq. (1). The heavy lines in Fig. 4(a) indicate that δ functions appear at these frequencies in the vibrational density of states (VDOS). The shaded areas indicate regions where states *may* exist.

Figure 4(b) is a schematic representation of the VDOS for the special case $\theta=120°$. The relative number of states between the band limits and in each δ function are shown

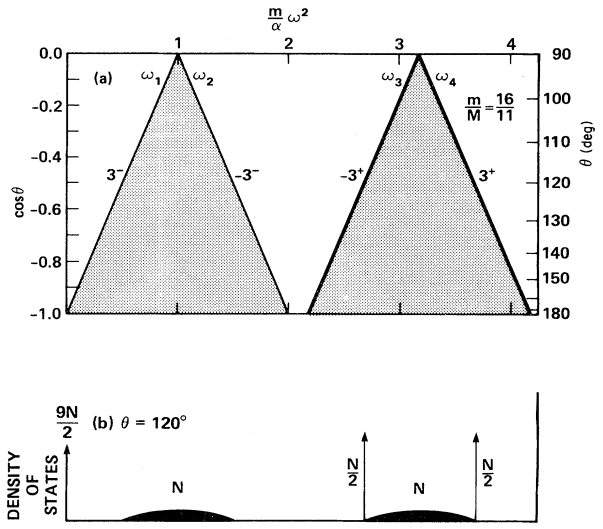

FIG. 4. Allowed frequency bands (a) for central-force vibrations of the network of planar AX_3 triangles shown in Fig. 3(a). States may exist in the shaded areas which are limited by the frequencies ω_1, ω_2, ω_3, and ω_4 that are determined by Eqs. (3). The heavy lines (ω_3 and ω_4) represent δ functions in the VDOS. Plot (b) is a schematic diagram of the VDOS for the network with $\theta=120°$; it shows the number of states in each band or δ function, where N is the total number of A (i.e., boron) atoms involved.

in the figure, and are calculated as follows. If the number of B atoms is N, then there is a total integrated weight of N in the density of states of the connectivity matrix, i.e., between the two limits of ϵ. The $\pm$ choice in Eq. (1) leads to two bands, each of weight N, as shown in Fig. 4(b). Of course, this is not all of the states: Some are in the δ functions at ω_3 and ω_4, while others are in the δ function at $\omega=0$, having been driven to zero frequency by the assumption that $\beta=0$. For N boron atoms, there are $3N/2$ oxygen atoms, giving a total of $5N/2$ atoms and $15N/2$ vibrational modes to be accounted for. In a central-force model, the total number of non-zero-frequency modes equals the number of *bonds*, $3N$. Since $2N$ modes are in the bonds, each of the δ functions must have $N/2$ states, as shown in Fig. 4(b). This leaves $(15/2)N-3N=(9/2)N$ modes at zero frequency, there being no restoring force for them in a central-forces-only model. These states actually occur at low but nonzero frequencies, as illustrated for v-SiO_2, v-GeO_2, and v-BeF_2 in Ref. 29, but they will not be further discussed in this paper.

The band limits in Fig. 4(b) for $\theta=120°$ and $m/M=16/11$ are given in dimensionless units by $(m/\alpha)\omega^2=0.5$ and 1.5; 2.688 and 3.688. We shall look at these limits later to see how they are modified by the inclusion of boroxol rings.

The fitting of Eqs. (3) to v-B_2O_3 data was discussed in detail in Ref. 23, which should be consulted. In short, the positions of the δ functions (ω_3 and ω_4) were equated with the observed high-frequency longitudinal-optical (LO) modes, and this allowed inversion of Eqs. 3(c) and 3(d) to yield experimental values of α and θ. These values were used to calculate the ω_1 and ω_2 using Eqs. 3(a) and 3(b).

TABLE I. Fit of Eqs. (3) to the v-B_2O_3 data, as described in the text and in Ref. 23. Here ω_3 and ω_4 are experimental frequencies (cm^{-1}), while α, θ, ω_2, and ω_1 are derived from them using Eqs. (3). Note that the predicted position of the uniform symmetric-stretch mode ($\omega_1=567$ cm^{-1}) is in poor agreement with the observed dominant Raman-line frequency ($\omega_R=808$ cm^{-1}). Reference 23 concluded that such a model *without regular rings* cannot fit the data.

ω_3	ω_4	α	θ	ω_2	ω_1	ω_R
1325	1550	612	120°	984	567	(808)

The results are restated in Table I. That the calculated frequency of the only "symmetric-stretch" motion (at $\omega_1=567$ cm^{-1}) was far removed from the dominant Raman line (at $\omega_R=808$ cm^{-1}) indicated that the model was inadequate.[23,27]

Also the Raman spectrum contained several more features than are suggested by Fig. 4(b). The failure of this simple model to account for most of the features of the spectrum is in stark contrast to the success of the same procedure when applied to several AX_2 tetrahedral glasses.[27,29] As we shall show, the principal problem is the absence of the boroxol rings from the assumed structure. It is perhaps encouraging that the best fit for ω_3 and ω_4 produces $\theta=120°$, which is precisely the value in a boroxol ring.

B. Network of threefold rings of planar AX_3 triangles

In this section we shall illustrate a particular method for creating a network of rings, for relating the eigenvalue spectrum of its connectivity matrix to a parent network not containing rings, and for calculating the band-frequency limits for central-force vibrations. While this will be done for the case of a network of boroxol-like rings, it should be clear how to use the methods to treat networks containing other kinds of rings.

Look carefully at the network of BO_3 triangles shown in Fig. 3(a). The replacement of each B atom by a more complex structure with the same trigonal bonding to the "outside" would obviously result in a network of the new structures. If each planar-connected B is replaced by a B_3O_3 planar ring, one obtains the network of boroxol-like rings shown in Fig. 5(a). The skeleton network of this system is shown in Fig. 5(b). It is a network of triangles, which could have been constructed directly from the skeleton network of Fig. 3(b) by replacing each three-connected vertex with a triangle, or threefold ring of vertices. This latter operation suggests that one might relate the connectivity matrix[2,28] of Fig. 5(b) to that of Fig. 3(b). In fact, one can easily relate the *eigenvalues* ϵ' of the connectivity matrix for Fig. 5(b) to those ϵ of the connectivity matrix For Fig. 3(b), as follows.

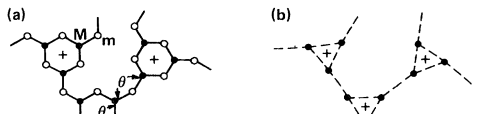

FIG. 5. Schematic (planarized) drawing of an idealized A_2X_3 network consisting of regular threefold-ring-like A_3X_6 units which share corners only. The $A-X-A$ angle θ is the same everywhere. There is no restriction on the dihedral angle (δ) at the X atoms which bridge between the A_3X_3 rings. Beyond the clearly defined A_3X_3 threefold rings the ring statistics are unspecified. The skeleton network for this structure is shown in (b), and is clearly based on triangles of A atoms. These *triangles* are the cause of new gaps and δ functions in the VDOS. Network (a) can be obtained from that of Fig. 3 by expanding each three-connected A atom in Fig. 3(a) into a three-connected A_3X_3 unit.

Consider the two skeleton networks, redrawn in Fig. 6. The symbols A_i, a_i, and b_i represent the amplitudes of energy eigenfunctions in the appropriate network. With the use of the notation of Weaire and Thorpe[28] and Fig. 6(a), Schrödinger's equation for single-nearest-neighbor interactions lead to the algebraic relation

$$\epsilon A_0=A_1+A_2+A_3\ . \tag{4}$$

That is, for single-nearest-neighbor interactions the energy ϵ of any collective excitation times its amplitude at one site A_0 is given by the sum of the amplitudes at the nearest-neighbor interacting sites.

A similar relation can be written for each eigenvalue ϵ' of the network of threefold rings in Fig. 6(b). Thus at site a_1

$$\epsilon' a_1=a_2+a_3+b_1 \tag{5}$$

or

$$(\epsilon'+1)a_1=A_0+b_1\ , \tag{6}$$

where we have used the fact that the total s-like part of the amplitude on a triangle in Fig. 6(b) is the same as the amplitude on the corresponding point in Fig. 6(a), i.e.,

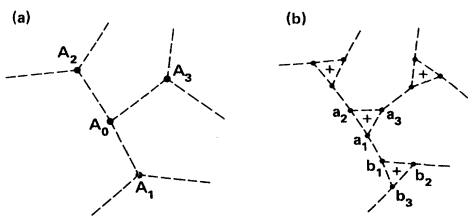

FIG. 6. Comparison of the *skeleton* networks of the two structural models introduced in Figs. 3 and 5, showing the labeling of the state amplitudes A_i, a_i, and b_i used in Eqs. (4)—(9). The skeleton network for the A_3X_3 ring model (b) can be derived directly from that for the AX_3 triangle model (a) by expanding each vertex in (a) into a triangle of vertices.

$$a_1+a_2+a_3=A_0,\quad b_1+b_2+b_3=A_1\ , \tag{7}$$

and so on. Similarly, we find that

$$(\epsilon'+1)b_1=A_1+a_1\ . \tag{8}$$

When we eliminate b_1 from Eqs. (6) and (8), we have

$$\epsilon'(\epsilon'+2)a_1=(\epsilon'+1)A_0+A_1\ . \tag{9a}$$

By inspection,

$$\epsilon'(\epsilon'+2)a_2=(\epsilon'+1)A_0+A_2\ , \tag{9b}$$

$$\epsilon'(\epsilon'+2)a_3=(\epsilon'+1)A_0+A_3\ . \tag{9c}$$

When Eqs. (9) are added, and combined with Eqs. (7) and (4), it follows that

$$\epsilon'(\epsilon'+2)=3(\epsilon'+1)+\epsilon \tag{10}$$

or

$$\epsilon'=\tfrac{1}{2}\pm(\epsilon+\tfrac{13}{4})^{1/2}\ . \tag{11}$$

From the bounds on ϵ [Eq. (2)], it follows that ϵ' is bounded by

$$-2\le\epsilon'\le 0\ , \tag{12}$$

$$1\le\epsilon'\le 3\ . \tag{13}$$

Thus there are two bands of eigenvalues for the connectivity matrix of the skeleton lattice in Fig. 5(b). The limiting values $\epsilon'=-2$, 0, 1, and 3 apply to any network of rings (planar or puckered) whose connectivity matrix corresponds to the topology of Fig. 5(b).

Thus we consider the ring network in Fig. 5(a) for the case that θ is the same *inside* and *outside* of the rings. This gives a network of *puckered* threefold rings. The special case $\theta=120°$ corresponds to a network of planar boroxol rings connected together by bridging oxygen atoms also having $\theta=120°$ (and unspecified values of δ). Since θ is thought to be $\sim 130°$ between the rings in v-B_2O_3,[17] the special case $\theta=120°$ is a useful approximate model.

When we assume that θ is the same inside and outside of the rings in Fig. 5(a), the central-force vibrational eigenfrequencies are still given by Eq. (1). This is because the central-force result is independent of *any* specific choice of dihedral angles, including the one that groups the triangles into rings as in Fig. 5(a). The band limits of the vibrational eigenfrequencies are found by substituting ϵ' into Eq. (1), whose quadratic nature doubles the number of limits to eight values, which we denote as -2^+, -2^-, 0^+, 0^-, 1^+, 1^-, 3^+, and 3^-. As before, the superscripts indicate the choice $\pm$ where it appears in Eq. (10). The band limits are plotted versus $\cos\theta$ in Fig. 7(a). The only straight lines versus $\cos\theta$ are the 3^-, -3^+, and 3^+ solutions of Eq. (1), and these are equal to ω_1^2, ω_3^2, and ω_4^2, respectively, as given in Eqs. (3).

The analysis thus far treats only the limiting values of the bands [shaded in Fig. 7(a)]. Note that the δ functions at frequencies labeled by -3^+ and $+3^+$ in the original network of triangles problem must be retained, and they behave with $\cos\theta$ just as before. That is, the effect of introducing threefold rings into the original network is to further limit the ranges of frequencies where there can be vibrational response. The original *bands* are broken up into subbands within the original limits. This means that the original δ *functions* survive. In addition, new δ functions may be created by the introduction of new order, and this is the case for our network of rings, as indicated by the heavy lines in Fig. 7(a) and by the schematic density of states for $\theta=120°$, shown in Fig. 7(b). Alternatively, we can say that the effect of introducing rings is to define *new gaps* and create *new* δ *functions* in the VDOS.

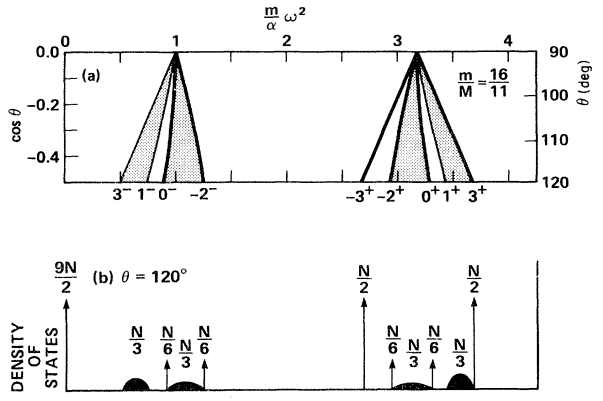

FIG. 7. Allowed frequency bands (a) for central-force vibrations of the network of A_3X_3 rings shown in Fig. 5(a). The frequency limits are labeled 3^-, 1^-, etc., as described in the text and as given by Eqs. (16)—(27) for the special case of $\theta=120°$. The schematic VDOS for $\theta=120°$ is shown in (b), where N is the number of A atoms in the structure. This VDOS is used to discuss isotope-shift data obtained on v-B_2O_3.

The counting of states is more difficult when the rings are introduced. We have arrived at the weights shown in Fig. 7(b) as follows. When we assume N boron atoms in the network of rings, there are still $3N/2$ oxygen atoms, a total of $5N/2$ atoms and $15N/2$ vibrational modes. The latter must still consist of $N/2$ states in each of the δ functions at $\epsilon=-3^+$ and $\epsilon=+3^+$, N states in the region between them, N states in the region between the limits at $\epsilon=3^-$ and -3^- and $9N/2$ states at zero frequency. [Compare Figs. 4(b) and 7(b).] The focus of the problem therefore is the redistribution of the N states within each of the two original allowed frequency ranges or "bands."

We first note that N boron atoms in the network of rings actually correspond to only $N/3$ boron atoms in the original network. This means that the number of states in the single band of the original skeleton network [Fig. 6(a)] leading to the present one [Fig. 6(b)] should be taken as $N/3$ states over the range given by Eq. (2). The quadratic nature of Eq. (11) means that $N/3$ states will lie in *each* of the two bands [defined by Eqs. (11) and (12)] for the connectivity matrix of the network of rings. Thus the *bands* in the connectivity matrix of the network of rings account for only $2N/3$ states, leaving $N/3$ states still to be accounted for. These are found in new δ functions whose origin is motion *inside* a ring (which has no analog in the motion of the single B atom of the original network whose expansion gave rise to the ring).

These new δ functions are understood as follows. We

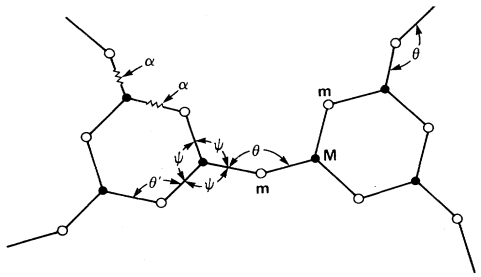

FIG. 8. Schematic (planarized) drawing of a more general A_2X_3 network consisting of regular A_3X_6 units which share corners only. This model is more general than that shown in Fig. 5(a) because the angles ψ around an A atom (●) are allowed to differ from 120°, and the central-force constants and $A-X-A$ angles within the ring (α',θ') are allowed to differ from those between the rings (α,θ). Again there is no restriction on the dihedral angles (δ) at the X atoms which bridge between the A_3X_3 rings.

first note that Eqs. (10) and (11) do not cover the case when all of the $A_i=0$ in Eqs. (9). The condition that $A_i=0$ corresonds to zero amplitude on *all* the boron atoms in the *original* network, and this occurs once each at ω_1 and ω_2. It also corresponds to zero total amplitude around each ring in the new network, i.e., $a_1+a_2+a_3=0$, etc. In Eqs. (9) we see that even for $A_i=0$, it is possible to have nonzero values of a_i, b_i, etc., at either of the two band limits, $\epsilon'=0$ and $\epsilon'=-2$. Equation (8) shows that when $A_i=0$ and $\epsilon'=0$ we have

$$b_i=a_i\ , \tag{14}$$

indicating that the amplitude on adjacent boron atoms in adjacent rings is the same [see Fig. 6(b)]. Similarly, Eq. (8) reveals that when $A_i=0$ and $\epsilon'=-2$ we have

$$b_i=-a_i\ , \tag{15}$$

indicating equal amplitudes of opposite phase on adjacent boron atoms in adjacent rings. We loosely refer to the states where $a_i=b_i$ as "bonding" states (with $\epsilon'=0$) and those where $a_i=-b_i$ as "antibonding" states (with $\epsilon'=-2$). There are $N/6$ of each, the two new δ functions thus accounting for the $N/3$ states not found in the bands delimited by Eqs. (12) and (13). This count can be verified by the following argument.[30] There are N-independent amplitudes, a_i, b_i, etc., in the new network of rings; $N/3$ constraints are required to make all $A_i=0$ and another $N/2$ constraints to make the state entirely bonding (or antibonding). This leaves $N-(N/3)-(N/2)=N/6$ degrees of freedom in the form of bonding (or antibonding) states. Thus there are $N/6$ states in each δ function at $\epsilon'=0$ and at $\epsilon'=-2$.

We emphasize that the new *skeleton* network contains *triangles* and *it is this fact* that leads to the dramatic changes in the eigenvalue spectrum of the connectivity matrix. The states near $\epsilon'=-3$ cannot be formed, as they would alternate $+1$, -1, $+1$, etc., from site to adjacent site and cannot be fit around the triangles. This also happens, although less dramatically, with any odd rings (e.g., fivefold rings). The δ functions at $\epsilon'=0$ and $\epsilon'=-2$ do not occur for squares, pentagons, etc. The eigenvectors consist of chains in Fig. 6(b) where the amplitude is $\ldots,+1,\ +1,\ -1,\ -1,\ +1,\ +1,\ -1,\ -1,\ldots$ for bonding states and $\ldots,+1,\ -1,\ +1,\ -1,\ +1,\ -1,\ +1,\ -1,\ldots$ for antibonding states, and zero away from the chain. Since v-B_2O_3 is believed to be based on threefold rings, it should show the above effects more dramatically than any other known glass.

We also comment that the transformation from ϵ to ϵ' could be repeated to ϵ'' by again replacing a B atom with a B_3O_3 ring. This could go on indefinitely in a hierarchical model until eventually the spectrum would consist only of δ functions and gaps. This is just a mathematical curiosity, of course, and would correspond to a fractal spectrum.

It is useful to evaluate the band-limit frequencies for the special case of $\theta=120°$ in Fig. 5(a). These are the baseline intercepts for $\cos\theta=-\frac{1}{2}$ in Fig. 7(a). We shall first define

$$y^2\equiv(m/\alpha)\omega^2\ , \tag{16}$$

$$A\equiv(3m/4M)+1\ , \tag{17}$$

and

$$B\equiv(3m/4M)^2+\tfrac{1}{4}\ . \tag{18}$$

It follows from Eq. (1) that

$$y^2(3^-)=\tfrac{1}{2}\ , \tag{19}$$

$$y^2(1^-)=A-[B+(m/4M)]^{1/2}\ , \tag{20}$$

$$y^2(0^-)=A-B^{1/2}\ , \tag{21}$$

$$y^2(-2^-)=A-[B-(m/2M)]^{1/2}\ , \tag{22}$$

$$y^2(-3^+)=\tfrac{1}{2}+(3m/2M)\ , \tag{23}$$

$$y^2(-2^+)=A+[B-(m/2M)]^{1/2}\ , \tag{24}$$

$$y^2(0^+)=A+B^{1/2}\ , \tag{25}$$

$$y^2(1^+)=A+[B+(m/4M)]^{1/2}\ , \tag{26}$$

$$y^2(3^+)=\tfrac{3}{2}+(3m/2M)\ . \tag{27}$$

These equations are relatively simple functions of the two masses involved, and will be used in Sec. III to compare with B and O isotopic substitution experiments on v-B_2O_3.

C. Network of threefold rings of puckered AX_3 triangles

We found it instructive to consider a more general central-force network problem where the force constants α' and angles θ' within the rings are allowed to be different than those (α,θ) between the rings. The variables are defined in Fig. 8 where for greater generality we have also allowed the O—B—O angle ψ to be different than 120°. When $\psi\neq120°$ the rings will necessarily be puckered[13,14] whatever the value of θ'. Of course, it is certain that $\psi=120°$ in v-B_2O_3,[19] while α' may be *smaller* than α by as much as 30%.[26]

In order to provide an independent check of the preceding section (which is a special case of the present problem), we did the derivation by the slightly different methods described in Ref. 2. Thus the problem was treated directly as a three-connected network of large vibrational units (puckered rings) whose connectivity matrix

has a single band of eigenvalues ϵ with the bounds ± 3 given in Eq. (2). For brevity we simply present the results without derivation.

We define dimensionless quantities as follows:

$$x^2 \equiv (m/\alpha)\omega^2 , \tag{28a}$$

$$x_i^2 \equiv (m/\alpha)\omega_i^2 \quad (i=1,2,3,4) , \tag{28b}$$

where

$$x_1^2 \equiv 1-\cos\theta'+(m/M)(1-\cos\psi) , \tag{29}$$

$$x_2^2 \equiv 1+\cos\theta'+(m/M)(1-\cos\psi) , \tag{30}$$

$$x_3^2 \equiv (\alpha'/\alpha)[1-\cos\theta+(m/M)(1-\cos\psi)] , \tag{31}$$

$$x_4^2 \equiv (\alpha'/\alpha)[1+\cos\theta+(m/M)(1-\cos\psi)] . \tag{32}$$

We next use these to define the following functions of ω^2.

$$L \equiv (\cos\psi)^{-1}-(2m/M)(x^2-x_1^2)^{-1} -(\alpha' m/\alpha M)(x^2-x_3^2)^{-1} , \tag{33}$$

$$M \equiv \cos\theta'(m/M)^2(x^2-x_1^2)^{-1}(x^2-x_2^2)^{-1} , \tag{34}$$

$$N \equiv \cos\theta(\alpha' m/\alpha M)^2(x^2-x_3^2)^{-1}(x^2-x_4^2)^{-1} . \tag{35}$$

The frequency limits associated with $\epsilon=-3$ are then given by the frequencies that solve

$$L = M \tag{36}$$

and also those that solve

$$L = 4M+2N . \tag{37}$$

Similarly, the limits associated with $\epsilon=+3$ are given by the frequencies that solve

$$L = 4M \tag{38}$$

and

$$L = M+2N . \tag{39}$$

In general, Eqs. (36)—(39) reduce to quartic polynomials in ω^2. Except for very limited cases, we have not been able to factor them, so they have been solved numerically for the roots of the polynomials involved. The solutions for $(m/M)=(16/11)$, $\alpha'=\alpha$, and $\theta'=\psi=120°$, are shown in Fig. 9(a), where as before, the heavy lines indicate the presence of δ functions in the VDOS. The only straight line is the δ function at 3.682, given by

$$(m/\alpha)\omega^2=(3/2)[1+(m/M)] . \tag{40}$$

Figure 9 constitutes the central-force results for a network of planar boroxol rings bridged by oxygen atoms at the common angle θ, and having identical B-O force constants α inside and outside the rings.

The schematic VDOS for this model of v-B_2O_3 with $\theta=130°$ is shown in Fig. 9(b), with the weights appropriate for N boron atoms. This should be compared with the result for $\theta=120°$, shown earlier in Fig. 7(b). Apart from

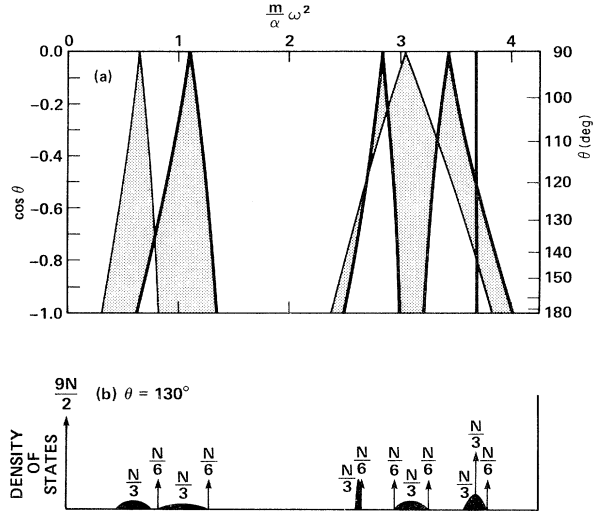

FIG. 9. Allowed frequency bands (a) for central-force vibrations of the more general network of AX_3 rings shown in Fig. 8(a). The frequency limits are shown for the special case $\psi=\theta'=120°$ and $\alpha'=\alpha$; they are the solutions of Eqs. (28)—(40). The schematic VDOS for $\theta=130°$ (between the rings) is shown in (b), where N is the number of A (boron) atoms in the structure. This VDOS is used to compare with the Raman data on v-B_2O_3, shown in Fig. 10(c).

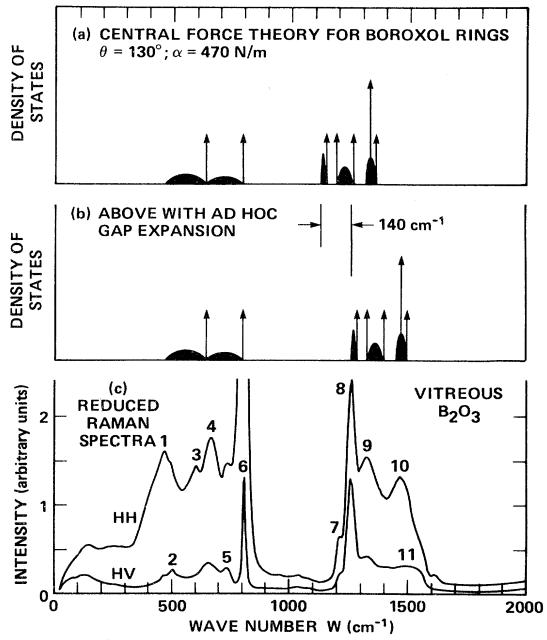

FIG. 10. Comparison of the Raman spectra of v-B_2O_3 (c) with a schematic representation (a) of the VDOS previously shown in Fig. 9(b) and calculated assuming the structural model shown in Fig. 8. The highly polarized Raman features marked 1 and 6 in (c) were fit to the high and low limits of the lower-frequency group of bands in (a) yielding $\alpha=470N/m$ and $\theta=130°$. In panel (b) an *ad hoc* shift of the high-frequency portion of (a) has been introduced, to help the reader to see the similarity of features with the corresponding part of the Raman spectra.

small shifts in band limits, the major change from $\theta=120°$ to $\theta=130°$ is the breakup of the two former δ functions having weight $N/2$. One of these becomes a δ function with weight $N/6$ and an accompanying band near 2.63; the other becomes a δ function with weight $N/6$ and an accompanying δ function (at 3.682) having weight $N/3$.

We note that the δ function at 3.682 has weight $N/3$, which is precisely the number of rings for N boron atoms. These states correspond to individually excited rings where the boron atoms "rotate" in one direction about the center of the ring and are perpendicular to the bonds connecting the ring to the rest of the network. For central forces only, this perpendicularity decouples the ring mode from the rest of the network. The oxygen atoms rotate in the opposite direction so that bonds around the ring are alternately stretched and compressed identically. With the use of arguments, developed elsewhere,[25,31] this means that the Raman activity of the mode will be *unpolarized*. We will therefore not further consider the mode.

The solutions of Eqs. (28)—(39) for the conditions of the earlier model in Sec. II B have been shown by numerical calculation to produce precisely the results shown in Fig. 7(a). This includes the results for $\theta=120°$ which are also given by Eqs. (16)—(27). In the latter case we understand the motions involved in one mode, the lowest-frequency band limit, 3^- in Fig. 7(a). This is a mode in which all B atoms remain at rest and all O atoms move in phase along the bisector of θ. As mentioned in Sec. II A this symmetric-stretch motion[27] will give highly polarized[25,31] Raman scattering with $I_{HH}\gg I_{HV}$. Unfortunately, we have not been able to clearly understand the motions for any other mode. This failure points to one of the shortcomings of the present method of determining band limits: There is no systematic machinery for calculating in an orderly fashion the vibrational eigenvectors corresponding to the band limits once the latter have been determined.

III. COMPARISON OF CENTRAL-FORCE THEORY WITH RAMAN SCATTERING IN v-B_2O_3

A. Spectral features

The richness of features in the VDOS due to rings [Fig. 9(b)] is in much better comparison with experiment than is that in the VDOS due to triangles [Fig. 4(b)]. We show this by direct comparison of the ring VDOS with the Raman spectra[23] shown in Fig. 10(c). The features in Fig. 10(c) are labeled 1—11 for easy reference. Only two parameters, α and θ, can be adjusted in order to fit the boroxol-ring theory of Fig. 9 to the data. This requires that any two features in the theoretical VDOS be identified with a correct pair of corresponding features in the Raman spectrum. Note that both theory and experiment consist of two groups of bands separated by a wide frequency gap.

We have chosen to fit to the two highly polarized bands labeled 1 and 6 in the lower-frequency portion of the Raman spectrum, as follows. As mentioned earlier, the lowest-frequency band edge in the theory is a *symmetric* stretch,[27] so it was made to coincide with the broad *highly* polarized line labeled 1 at $\sim 470\ \mathrm{cm}^{-1}$ in the Raman spectrum.[25,31] The highest-frequency band edge below the wide gap in the theory coincides with a δ function and therefore was made to fit the sharp highly polarized line labeled 6 just below the band gap in the Raman spectrum. These conditions determine that $\theta=130°$ and $\alpha=470n/m$; the boroxol-ring model VDOS for these parameters is plotted in Fig. 10(a).

In Fig. 10(b) we introduce an *ad hoc* expansion of the gap, in order to emphasize the favorable comparison of the theoretical features with corresponding peaks in the Raman spectra of Fig. 10(c). Much of this gap expansion would be accounted for by allowing α to be appreciably larger than α'. We have not carried out this additional

TABLE II. Theoretical boron and oxygen isotope shifts for v-B_2O_3, according to the simplified planar-ring model with all B—O—B angles $\theta=120°$. The features are labeled as in Fig. 7(a). The fractional shifts $\Delta\omega/\omega$ given below were calculated using Eqs. (19)—(27) for two cases: (a) boron substitution, $^{10}B\rightarrow{}^{11}B$ (with $M_O=16$); (b) oxygen substitution, $^{16}O\rightarrow{}^{18}O$ (with $M_B=11$). Note that the predicted fractional shifts tend to group into two values for each substitution, one below the frequency gap and another above the gap. It is these nearly constant values that are compared with experiment in Tables III and IV.

Feature label	Type of feature	(a) Boron $\dfrac{\omega_{^{11}B_2O_3}-\omega_{^{10}B_2O_3}}{\omega_{^{10}B_2O_3}}$	(b) Oxygen $\dfrac{\omega_{B_2{}^{18}O_3}-\omega_{B_2{}^{16}O_3}}{\omega_{B_2{}^{16}O_3}}$
3^-	Raman edge	0	−0.057
1^-	band edge	−0.004	−0.052
0^-	δ function	−0.005	−0.051
-2^-	δ function	−0.004	−0.053
	Frequency gap		
-3^+	δ function	−0.038	−0.010
-2^+	δ function	−0.034	−0.016
0^+	δ function	−0.030	−0.020
1^+	band edge	−0.030	−0.022
3^+	δ function	−0.028	−0.023

TABLE III. Experimental $^{10}B \rightarrow {}^{11}B$ isotope shifts in high-purity v-B_2O_3. The features are as labeled in Fig. 10(c). The frequencies (cm^{-1}) in columns (a) and (b) were reported by Galeener and Geissberger (Ref. 32), as were the shifts Δ ($=\omega_{^{11}B_2O_3}-\omega_{^{10}B_2O_3}$) in column (c). The shifts in column (d) were reported by Windisch and Risen (WR) (Ref. 33). The average of columns (c) and (d) is Δ_B [$=\frac{1}{2}(\Delta+\Delta_{WR})$] given in column (e). The uncertainties in Δ_B given in column (f) are derived from those given in Ref. 32, on the assumption that the uncertainties in Δ_{WR} are the same as reported for Δ. The observed fractional change in Δ_B is given in column (g), where those values which compare well with the central-force theoretical results in Table II are enclosed in square brackets. We conclude that features 4—8 require the addition of noncentral forces to the theory.

Feature	(a) $\omega_{^{11}B_2O_3}$	(b) $\omega_{^{10}B_2O_3}$	(c) Δ	(d) Δ_{WR}	(e) Δ_B	(f) Uncertainty	(g) $\Delta_B/\omega_{^{10}B_2O_3}$
1	470	470	0	−2	−1	(±3)	[−0.002]
2	502	506	−4	0	−2	(±3)	[−0.004]
3	602	606	−6	−1	−4	(±3)	[−0.005]
4	660	681	−21	−18	−20	(±3)	−0.029
5	732	750	−18	−28	−23	(±4)	−0.031
6	809	808	+1	0	0	(±1)	0
			Frequency gap				
7	1212	1236	−24	−30	−27	(±6)	−0.022
8	1261	1288	−27	−24	−26	(±3)	−0.020
9	1327	1371	−44	−44	−44	(±6)	[−0.032]
10	1467	1510	−43	−49	−46	(±6)	[−0.030]
11	1510	1555	−45	· · ·	−45	(±8)	[−0.029]

complication because the fitting procedure would be tedious, and because we will shortly show that errors due to the omission of noncentral forces (β) may be just as important.

B. Isotope shifts

Galeener and Geissberger[32] have reported measurements of the $^{10}B \rightarrow {}^{11}B$ isotope shifts in v-B_2O_3, and have found shifts of zero (± 1 cm^{-1}) for the lines marked 1 and 6 in Fig. 10(c). Similar results have been reported by Windisch and Risen[33] who also measured the $^{16}O \rightarrow {}^{18}O$ isotope shifts. We can test some aspects of our central-force ring model by comparing calculated isotope shifts with the above measurements.

We shall use the simplified planar-ring model derived in Sec. II B, in which the B—O—B angle θ is 120° everywhere. The schematic density of states shown in Fig. 7(b) is similar to that for the more general model with $\theta = 130°$ outside the rings, seen in Fig. 9(b). We use the simpler model because the isotope shifts of the band limits can be easily calculated using Eqs. (19)—(27). The results are

TABLE IV. Experimental $^{16}O \rightarrow {}^{18}O$ isotope shifts in high-purity v-B_2O_3. The features are as labeled in Fig. 10(c). The frequencies (cm^{-1}) in columns (a) and (b) were reported by Windisch and Risen (Ref. 33), as were the shifts Δ_O ($=\omega_{B_2{}^{18}O_3}-\omega_{B_2{}^{16}O_3}$) in column (c). The feature-by-feature uncertainties were not given in Ref. 33, and are here taken to be the same as listed in Table III. The observed fractional change in Δ_O is given in column (d), where those values which compare well with the central-force theoretical results in Table II are enclosed in square brackets. As in Table III, we conclude that features 4—8 require the addition of noncentral forces to the theory. We are unable to explain why features 9 and 10 disagree with theory here, but not in Table III.

Feature	(a) $\omega_{B_2{}^{18}O_3}$	(b) $\omega_{B_2{}^{16}O_3}$	(c) Δ_O	(d) $\Delta_O/\omega_{B_2{}^{16}O_3}$
1	445	470	−25	[−0.053]
2	472	500	−28	[−0.056]
3	570	605	−35	[−0.058]
4	657	661	−4	−0.006
5	· · ·	732	· · ·	· · ·
6	760	808	−48	−0.059
		Frequency gap		
7	1176	1208	−32	−0.026
8	1235	1260	−25	−0.020
9	1320	1329	−9	−0.007
10	1445	1460	−15	−0.010
11	· · ·	· · ·	· · ·	· · ·

given in Table II, where the features are labeled as in Fig. 7(a). We have calculated the percent change in frequency going from the lighter to the heavier mass for both boron substitution [column (a)] and oxygen substitution [column (b)]. The *percent change* $\Delta\omega/\omega$ facilitates comparison with experiment.

Table II shows that $\Delta\omega/\omega$ for boron substitution varies from zero to about -0.005 for the low-frequency group (3^-, 1^-, 0^-, 2^-) and is near -0.032 for the high-frequency group (-3^+, -2^+, 0^+, 1^+, 3^+). For oxygen substitution, $\Delta\omega/\omega$ is near -0.053 over the low frequencies, and increases from -0.010 to -0.023 over the high frequencies. We shall compare these numbers against percent frequency shifts measured in the low- and high-frequency regions of the observed spectra.

The experimental $^{10}B\rightarrow{}^{11}B$ isotope shift data are presented in Table III, with details discussed in the table heading. The experimental features are labeled 1—11 as was defined in Fig. 10(c), and the frequency gap is between features 6 and 7. The average observed shifts Δ_B are given in column (e), and the percent shifts ($\Delta_B/\omega_{^{10}B_2O_3}$) in column (g). Those features in the low-frequency region (1—6) whose percent shifts compare well with the range of theoretical values in the low-frequency region of column (a) in Table II are enclosed in square brackets in column (g) of Table III. *That is, the square brackets indicate that the observed shift is of the size predicted by the central-force network of rings.*

The shifts in features 4 and 5 of Table III are much too *large* to be explained by our present theory. This suggests the involvement of more boron motion than exists in any low-frequency mode of the theory. We propose that features 4 and 5 are modes of the ring in which B and O atoms move out of the plane of the ring. Since restoring forces for such motions can be obtained only by including noncentral forces, these motions are completely absent from our model. Also, since at least these two of the six low-frequency features cannot be predicted by the central-force theory it is clearly premature to attempt an *optimum* fit to the data by using $\alpha'\neq\alpha$, $\theta'\neq\theta$, etc., as allowed by the more general central-force ring results presented in Sec. II C.

The shifts in features 7 and 8 are too *small* to be explained by our present theory. This suggests the involvement of more oxygen motion than exists in any high-frequency mode of the theory. In this case, we suspect that the modes already exist in our calculations but that their frequencies, and the extent of involvement of oxygen motion, are substantially altered by the inclusion of noncentral forces. Again, the corrected modes may involve motion out of the plane of the ring.

The experimental $^{16}O\rightarrow{}^{18}O$ isotope-shift data are presented in Table IV. As before we conclude that the shifts of features 4, 5, 7, and 8 are not consistent with the simple central-force ring theory, and that they are likely to be explained upon introduction of noncentral forces into the theory. Table IV also shows that the oxygen shifts of features 9 and 10 do not agree with the central-force ring theory. This is puzzling since their boron shifts are well predicted and since the central-force theories have previously predicted isotope shifts especially well at the highest frequencies.[34–36]

The B and O isotope shifts of feature 6 are also outside of theoretical predictions, but the discrepancies are small. On the other hand, the discrepancies are completely removed if we simply assume that there is oxygen motion only, for which $\Delta_B=0$ and $\Delta_O=-46$ cm^{-1}. This suggests that the central face theory includes too much B motion in feature 6.

In general, it appears that the inclusion of noncentral forces in the ring-network model for v-B_2O_3 will alter several frequencies by amounts which are not necessarily small compared to the separation of neighboring features in Figs. 7(b) or 9(b). We think it unlikely that the identification of experimental feature 1 in Fig. 10(c) with the uniform symmetric stretch [solution 3^- in Fig. 7(a)] will change, especially because the observed boron isotope shift is very near the predicted zero value. That the dominant Raman line (feature 6) shows a boron isotope shift (0 ± 1 cm^{-1}) that is definitely smaller than predicted ($-0.004\times808\simeq-3$ cm^{-1}) may indicate that the mode order will be changed when $\beta\neq0$ are introduced. Presently, we speculate that $\beta\neq0$ will "stiffen" the ring, leading to less B motion and a smaller predicted isotope shift.

IV. SUMMARY AND CONCLUDING COMMENTS

We have derived the band limits in the central-force approximation for a network of planar or puckered threefold A_3X_3 rings, suitable for discussion of the vibrational frequencies of v-B_2O_3 (in the boroxol-ring model). The schematic diagram of the VDOS for a network of planar AX_3 units containing no rings is reproduced in Fig. 11(a). The effect of expanding each B-atom vertex into a (planar) threefold A_3X_3 ring is shown by the schematic diagram reproduced in Fig. 11(b). Comparison of these diagrams shows that the introduction of rings (triangles in the skeleton network) is to produce new gaps in the possible regions of vibrational frequencies, and to introduce additional δ functions in the VDOS. Thus the connectivity associated with threefold rings is alone capable of increasing

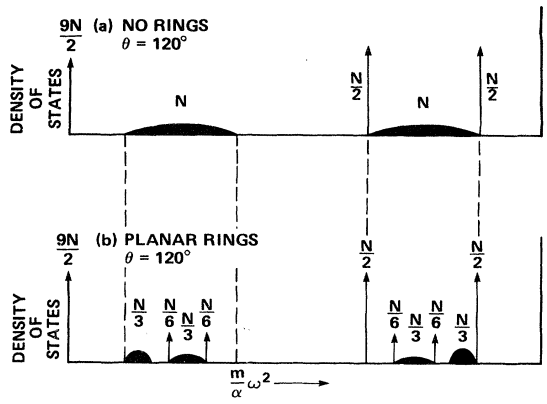

FIG. 11. Comparison of the schematic VDOS for a network of planar AX_3 units with no ring specification (a) and those for a similar network of planar A_3X_3 (boroxol) *rings* (b). The qualitative effect of introducing threefold rings is profound, giving rise to an increase in the main band gap, the introduction of new gaps, and the introduction of new δ functions.

the gap between low- and high-frequency regions, as illustrated in Fig. 11. This increased gap and the new richness of spectral structure enable the network of rings model to compare qualitatively quite well with the observed Raman spectra, as was illustrated in Fig. 10. This lends support to the boroxol-ring model as an explanation of the structure and vibrations of v-B_2O_3.

The boron and oxygen isotope shifts of the band limits in the network of rings model were calculated (Table II) and compared with experimental observations (Tables III and IV). For most observed lines the agreement was good. However, the features marked 4, 5, 7, and 8 in Fig. 10(c) were poorly fit to the theory, and we believe that their correct explanation requires introduction of noncentral force, not used in the present ring theory. In particular, features 4 and 5 may be out-of-plane motions of the atoms in the ring, and these have no restoring force in the central-forces-only model.

We concluded that the broad highly polarized line at 470 cm^{-1} [feature 1 in Fig. 10(c)] is associated with symmetric-stretch motions of the oxygen atoms that bridge between the rings in v-B_2O_3. The breadth of the line is due to the spread in this bridging oxygen angle. In Fig. 10 (Sec. III A) the fit to our ring theory determined that the most probable value for this B—O—B angle is 130°, the same value that has been deduced from diffraction experiments.[17]

We also conclude that the sharp highly polarized line at 808 cm^{-1} [feature 6 in Fig. 10(c)] is associated with symmetric-stretch motions of the oxygen atoms inside the rings in v-B_2O_3. These motions have been described as a breathing mode of the boroxol ring by several previous authors.[26,33,35] The complete absence of a B isotope shift indicates that there is very little B motion in this breathing mode.[35] The sharpness of the line is due to the *lack* of spread in the angle at the moving oxygen, which is uniformly 120° in the ring.

We were able to understand the motions in only one other mode of the model, the high-frequency δ function with weight $N/3$ in Fig. 9(b), or Fig. 10(b). This is the counter-rotating ring mode described near the end of Sec. II C. In central forces only, each of these modes is completely localized to a different *one* of the $N/3$ rings. Since the mode is not expected to be highly polarized it may be associated with the feature labeled 11 (rather than 10) in the Raman spectrum of Fig. 10(c).

On the whole, the inclusion of planar boroxol rings in the central-force model for vibrations in v-B_2O_3 produces much better agreement with the Raman experiments. A similar qualitative conclusion was reached using large cluster calculations by Bell and Carnevale.[24] Our isotope-shift study provides strong indications that the inclusion of noncentral forces will lead to an improved quantitative description. We thus recommend several improvements for future work: (1) the inclusion of noncentral forces, (2) the development of a *method* for deducing the atomic motions involved, and (3) a treatment of the relatively small, but nonzero TO-LO splittings[37,38] reported in Ref. 23. It appears that a homogeneous model of rings bridged by oxygen atoms, not BO_3 triangles or more complicated units, will suffice. This suggests the use of a Bethe lattice[39,40] of boroxol rings with central and noncentral forces, since such calculations on an "infinite structure" can easily give the resolution needed to check isotope-shift data.

This work has demonstrated, for the first time, how increased structure arises in the vibrational spectra of glasses as the order is extended beyond the range of immediate nearest neighbors to include rings. This is a very general result.

ACKNOWLEDGMENTS

The authors are grateful to the U.S. Navy Office of Naval Research (through G. B. Wright) for suppport of this work under Contracts Nos. N00014-80-C-0713 and N00014-80-C-0610. We are also grateful to Dr. A. E. Geissberger for a critical reading and discussion of the manuscript. One of us (M.F.T.) would like to thank the Xerox Palo Alto Research Center for their hospitality.

*Address until 31 October 1984: University of Cambridge, Cavendish Laboratory, Madingley Road, Cambridge, CB3 OHE, U.K.

†Permanent address: Physics Department, Michigan State University, East Lansing, MI 48824.

[1]P. N. Sen and M. F. Thorpe, Phys. Rev. B 15, 4030 (1977).

[2]M. F. Thorpe and F. L. Galeener, Phys. Rev. B 22, 3078 (1980).

[3]M. F. Thorpe and D. Weaire, Phys. Rev. Lett. 23, 1581 (1971).

[4]J. D. Joannopoulos and M. L. Cohen, Phys. Rev. B 7, 2644 (1973).

[5]J. A. Blackman and M. F. Thorpe, Phys. Rev. B 23, 2871 (1980).

[6]For a more complete set of references, see J. Singh, Phys. Rev. B 23, 4156 (1981).

[7]For a summary, see A. C. Wright and J. A. Erwin Desa, Phys. Chem. Glasses 19, 140 (1978). See also Table IV of G. Etherington, A. C. Wright, J. T. Wenzel, J. C. Dore, J. H. Clarke, and R. N. Sinclair, J. Non-Cryst. Solids 48, 265 (1982).

[8]R. J. Bell and P. Dean, Philos. Mag. 25, 1381 (1972).

[9]D. E. Polk, J. Non-Cryst. Solids 5, 365 (1971).

[10]G. A. N. Connell and R. J. Temkin, Phys. Rev. B 9, 5323 (1974).

[11]See, e.g., W. Paul and G. A. N. Connell, in *Physics of Structurally Disordered Solids*, edited by S. S. Mitra (Plenum, New York, 1980), p. 45.

[12]W. H. Zachariasen, J. Am. Chem. Soc. 54, 3841 (1932).

[13]F. L. Galeener, J. Non-Cryst. Solids 49, 53 (1982).

[14]F. L. Galeener, Solid State Commun. 44, 1037 (1982).

[15]J. Goubeau and H. Z. Keller, Inorg. Chem. 272, 303 (1953).

[16]J. Krogh-Moe, J. Non-Cryst. Solids 1, 269 (1969).

[17]R. L. Mozzi and B. E. Warren, J. Appl. Crystallogr. 3, 251 (1970).

[18]G. E. Jellison, Jr., L. W. Panek, P. J. Bray, and G. B. Rouse, Jr., J. Chem. Phys. 66, 802 (1977); P. J. Bray, S. A. Feller, G. E. Jellison, Jr., and Y. H. Yun, J. Non-Cryst. Solids 38-39, 93 (1980).

[19]A. H. Silver and P. J. Bray, J. Chem. Phys. 29, 984 (1958); S. E. Svanson, E. Forslind, and J. Krogh-Moe, J. Phys. Chem. 66, 174 (1962).
[20]S. R. Elliott, Philos. Mag. B 37, 435 (1978).
[21]D. L. Griscom, in *Borate Glasses,* edited by L. D. Pye, V. D. Frechette, and N. J. Kreidl (Plenum, New York, 1978), p. 11.
[22]P. A. V. Johnson, A. C. Wright, and R. N. Sinclair, J. Non-Cryst. Solids 50, 281 (1982).
[23]F. L. Galeener, G. Lucovsky, and J. C. Mikkelsen, Jr., Phys. Rev. B 22, 3983 (1980).
[24]R. J. Bell and A. Carnevale, Philos. Mag. B 43, 389 (1981).
[25]R. M. Martin and F. L. Galeener, Phys. Rev. B 23, 3071 (1981).
[26]T. W. Bril, Philips Res. Rep. Suppl. No. 2, 1 (1976).
[27]F. L. Galeener, Phys. Rev. B 19, 4292 (1979).
[28]D. Weaire and M. F. Thorpe, in *Computational Methods for Large Molecules and Amorphous Semiconductors,* edited by F. Herman, A. D. McLean, and R. K. Nesbet (Plenum, New York, 1972), p. 295.
[29]F. L. Galeener, A. J. Leadbetter, and M. W. Stringfellow, Phys. Rev. B 27, 1052 (1983).
[30]This type of argument was used in Ref. 28.
[31]F. L. Galeener, J. Phys. (Paris) Colloq. 42, C6-24 (1981).
[32]F. L. Galeener and A. E. Geissberger, J. Phys. (Paris) Colloq. 44, C9-343 (1983).
[33]C. F. Windisch and W. M. Risen, Jr., J. Non-Cryst. Solids 48, 307 (1982).
[34]F. L. Galeener and J. C. Mikkelsen, Jr., Phys. Rev. B 23, 5527 (1981).
[35]F. L. Galeener and A. E. Geissberger, Phys. Rev. B 27, 6199 (1983).
[36]F. L. Galeener, A. E. Geissberger, G. W. Ogar, Jr., and R. E. Loehman, Phys. Rev. B 28, 4768 (1983).
[37]F. L. Galeener and G. Lucovsky, Phys. Rev. Lett. 37, 1474 (1976).
[38]F. L. Galeener, G. Lucovsky, and R. H. Geils, Solid State Commun. 25, 405 (1978).
[39]R. B. Laughlin, J. D. Joannopoulos, C. A. Murray, K. J. Hartnett, and T. J. Greytak, Phys. Rev. Lett. 40, 461 (1978).
[40]For a general discussion of Bethe-lattice applications, see M. F. Thorpe, in *Excitations in Disordered Systems,* edited by M. F. Thorpe (Plenum, New York, 1982), p. 85.